

Effects of initial electronic state on vortex patterns in counter-rotating circularly polarized attosecond pulses

Qi Zhen(甄琪), Jia-He Chen(陈佳贺), Si-Qi Zhang(张思琪), Zhi-Jie Yang(杨志杰), and Xue-Shen Liu(刘学深)†

Citation: Chin. Phys. B, 2021, 30 (**2**): 024203. DOI: 10.1088/1674-1056/abb7fb
Journal homepage: http://cpb.iphy.ac.cn; http://iopscience.iop.org/cpb

What follows is a list of articles you may be interested in

Photoelectron momentum distributions of single-photon ionization under a pair of elliptically polarized attosecond laser pulses

Hui-Fang Cui(崔会芳), Xiang-Yang Miao(苗向阳)
Chin. Phys. B, 2020, 29 (**7**): 074203. DOI: 10.1088/1674-1056/ab8ac0

Inhibiting radiative recombination rate to enhance quantum yields in a quantum photocell

Jing-Yi Chen(陈镜伊), Shun-Cai Zhao(赵顺才)
Chin. Phys. B, 2020, 29 (**6**): 064207. DOI: 10.1088/1674-1056/ab836f

Oxide-aperture-dependent output characteristics of circularly symmetric VCSEL structure

Wen-Yuan Liao(廖文渊), Jian Li(李健), Chuan-Chuan Li(李川川), Xiao-Feng Guo(郭小峰), Wen-Tao Guo(郭文涛), Wei-Hua Liu(刘维华), Yang-Jie Zhang(张杨杰), Xin Wei(韦欣), Man-Qing Tan(谭满清)
Chin. Phys. B, 2020, 29 (**2**): 024201. DOI: 10.1088/1674-1056/ab5fbd

Influence of intraband motion on the interband excitation and high harmonic generation

Rui-Xin Zuo(左瑞欣), Xiao-Hong Song(宋晓红), Xi-Wang Liu(刘希望), Shi-Dong Yang(杨士栋), Wei-Feng Yang(杨玮枫)
Chin. Phys. B, 2019, 28 (**9**): 094208. DOI: 10.1088/1674-1056/ab3446

Reduced graphene oxide as saturable absorbers for erbium-doped passively mode-locked fiber laser

Zhen-Dong Chen(陈振东), Yong-Gang Wang(王勇刚), Lu Li(李璐), Rui-Dong Lv(吕瑞东), Liang-Lei Wei(韦良雷), Si-Cong Liu(刘思聪), Jiang Wang(王江), Xi Wang(王茜)
Chin. Phys. B, 2018, 27 (**8**): 084206. DOI: 10.1088/1674-1056/27/8/084206

Effects of initial electronic state on vortex patterns in counter-rotating circularly polarized attosecond pulses*

Qi Zhen(甄琪), Jia-He Chen(陈佳贺), Si-Qi Zhang(张思琪),
Zhi-Jie Yang(杨志杰), and Xue-Shen Liu(刘学深)†

Institute of Atomic and Molecular Physics, Jilin University, Changchun 130012, *China*

(Received 11 August 2020; revised manuscript received 1 September 2020; accepted manuscript online 14 September 2020)

We theoretically investigate the effects of different electronic states as the initial state on the vortex patterns in photoelectron momentum distributions (PMDs) from numerical solutions of the two-dimensional (2D) time-dependent Schrödinger equation (TDSE) of He^+ with a pair of counter-rotating circularly polarized attosecond pulses. It is found that the number of spiral arms in vortex patterns is equal to the number of the absorbed photons when the initial state is the ground state. However, the number of spiral arms in vortex patterns is always two more than the number of the absorbed photons when the initial state is the excited state. This sensitivity is attributed to the initial electron density distribution. In addition, we have demonstrated the PMDs for different initial electronic states with the same wavelengths and analyzed their corresponding physical mechanisms. It is illustrated that the method presented can be employed to effectively control the distribution of the electron vortices.

Keywords: initial electronic state, counter-rotating circularly polarized attosecond pulses, vortex patterns, photoelectron momentum distributions

PACS: 42.50.Hz, 42.65.Ky, 32.80.Rm **DOI:** 10.1088/1674-1056/abb7fb

1. Introduction

The rapid development of ultrashort laser pulses provides new tools for exploring electronic dynamics on the attosecond (1 as $= 10^{-18}$ s) time scale.[1–3] To date, the shortest single pulse with duration 43 as has been produced from superposing some orders of the high-order harmonics generation,[4] which can be used to monitor pure electronic quantum effects through attosecond imaging.[5] The ultrashort attosecond pulses can also induce electron charge migration, thus offering the possibility for probing the molecular structure and imaging the molecular reactions.[6–8]

In the research, a variety of pulses and their combinations have been used to explore electron dynamics, including the high-order harmonic generation (HHG),[9–14] nonsequential double ionization (NSDI),[15–18] and the photoelectron momentum distribution (PMD).[19–23] Recently it was found that single ionization of atom by two oppositely circularly polarized, time-delayed attosecond pulses produce vortex patterns in PMDs,[24–27] which are sensitive to the time delay between the pulses, their handedness, and their relative phase. Yuan *et al.*[28,29] theoretically investigated the dependence of vortex patterns in PMDs on molecular geometry by bichromatic circularly polarized attosecond laser pulses. Li *et al.*[30] explored the symmetry distortion of the vortex patterns by considering the dynamic Stark effect and demonstrate that the vortex patterns can also be generated by a pair of elliptically polarized laser pulses.[31] Experimentally, the electron vortices of the potassium atom in counter-rotating circularly polarized laser fields were produced and manipulated, and the experimental results are in identical with the results of numerical simulation.[32,33] In 2019, Xiao *et al.*[34] demonstrated a scheme to accurately measure the electron displacement using a ruler formed by vortex patterns in PMDs generated by two oppositely circularly polarized pulses.

In this paper, we investigate the effects of different initial electronic states on the vortex patterns in counter-rotating circularly polarized laser pulses. The numerical results of PMDs were presented with varying the wavelengths of attosecond laser pulses. The results show that the vortex patterns in PMDs are dependent on the initial electron density distribution. Besides, we compare the PMDs of different initial electronic states with the same wavelengths and discuss the corresponding physical mechanisms of the discrepancy in distribution.

We divide the paper into the following parts. Our theoretical model and computational method are given in Section 2. The numerical results of PMDs with the different electronic state as the initial state are presented and discussed in Section 3. Finally, we make a summary in Section 4. Atomic units (a.u.) $e = \hbar = m_e = 1$ are used unless otherwise stated.

2. Theoretical methods

To illustrate the effects of the ground and first excited states as the initial electronic state on the vortex patterns in PMDs, we solve the two-dimensional (2D) time-dependent

*Project supported by the National Natural Science Foundation of China (Grant No. 12074142), the Natural Science Foundation of Jilin Province of China (Grant No. 20180101225JC), and the Graduate Innovation Fund of Jilin University, China (Grant No. 101832020CX337).

†Corresponding author. E-mail: liuxs@jlu.edu.cn

© 2021 Chinese Physical Society and IOP Publishing Ltd

Schrödinger equation (TDSE) of the He^+ with a pair of counter-rotating circularly polarized pulses. The 2D TDSE under the dipole approximation and the length gauge is

$$i\frac{\partial\psi(\boldsymbol{r},t)}{\partial t}=\left[\frac{\boldsymbol{p}^2}{2}+V(\boldsymbol{r})+\boldsymbol{r}\cdot\boldsymbol{E}(t)\right]\psi(\boldsymbol{r},t), \tag{1}$$

where $\boldsymbol{r}$ and $\boldsymbol{p}$ are the coordinate and the momentum operator of the electron, respectively; The soft-core Coulomb potential is

$$V(\boldsymbol{r})=-\frac{b}{\sqrt{r^2+a}}. \tag{2}$$

The soft-core parameters $a=0.161$ and $b=2.0$, which corresponds to the ionization potential $I_{P_1}=2$ a.u. of the ground state and $I_{P_2}=0.5$ a.u. of the first excited state of He^+. $\boldsymbol{E}(t)$ is the electric field of a pair of counter-rotating circularly polarized pulses delayed in time by T_d,

$$\boldsymbol{E}(t)=\boldsymbol{E}_1(t)+\boldsymbol{E}_2(t), \tag{3}$$

with

$$\boldsymbol{E}_1(t) = E_0 f(t)\left[\hat{e}_x\cos(\omega_1 t)+\hat{e}_y\sin(\omega_1 t)\right], \tag{4}$$

$$\boldsymbol{E}_2(t) = E_0 f(t+T_d)\{\hat{e}_x\cos\left[\omega_2(t+T_d)\right] - \hat{e}_y\sin\left[\omega_2(t+T_d)\right]\}, \tag{5}$$

where the amplitude of the laser pulse is $E_0=0.11$ a.u. ($I_0=4\times10^{14}$ W/cm^2); $\omega_{1/2}$ is the laser angular frequency. The envelope of the laser pulse is $f(t)=\exp\left[-4(\ln2)t^2/\tau^2\right]$, and the full width at half-maximum (FWHM) is $\tau=2T$ ($T=2\pi/\omega_1$).

The research is based on solving the 2D TDSE by the fast Fourier transform technique combined with the split-operator method.[35] We utilize the imaginary-time evolution method to obtain the initial wave function. The grid size is 409.6 a.u. containing 2048 grid points in both x and y directions. The wave packet at each step is multiplied by a $\cos^{1/8}$ "mask function", which is used to prevent unphysical effects from the boundary. Thus, the absorber domain ranges from $|x,y|=150$ a.u. to $|x,y|=204.8$ a.u. At final propagation time, the wave packet is multiplied by a mask function $M(r)$, which divides the wave packet into the bounded part and ionized part.[20,36] The PMDs is obtained by Fourier transforming the wave packet of the ionized part.

3. Results and discussion

To investigate the effects of different initial electronic states on the vortex patterns, we present the PMDs of He^+ with varying the wavelengths of the time-delayed attosecond pulses. Figures 1(a)–1(c) display the PMDs of the vortex patterns at the different wavelengths for the time delay $T_d=3$ o.c. for the ground state as the initial electronic state.

Figure 1(a) displays that the vortex pattern in PMDs exhibit two spiral arms at wavelengths $\lambda_1=\lambda_2=20$ nm ($\omega_1=\omega_2=2.28$ a.u.). We can see that there are four interference spiral arms at wavelengths $\lambda_1=\lambda_2=40$ nm ($\omega_1=\omega_2=1.14$ a.u.) as shown in Fig. 1(b), whereas eight spiral arms are induced at wavelengths $\lambda_1=\lambda_2=90$ nm ($\omega_1=\omega_2=0.5$ a.u.) as shown in Fig. 1(c). We also found that each spiral arm is evenly separated by the same angle as shown in Figs. 1(a)–1(c). The similar distribution patterns of H_2^+ have been discussed systematically in Ref. [29].

The physical mechanism underlying the generation of electron vortices is the superposition of two time delayed photoelectron wave packets with different magnetic quantum number m.[25,32] In Figs. 1(a)–1(c), the photoelectron wave packets are generated by the ionization of ground state He^+ with a left-right circularly polarized attosecond pulses. In Fig. 1(a), the wavelengths of both laser pulses are $\lambda_1=\lambda_2=20$ nm ($\omega_1=\omega_2=2.28$ a.u.), which are above the ionization potential of the ground state of He^+ ($I_{P_1}=2$ a.u.). The electrons can be ionized by absorbing one photon. Thus, the first left-handed circularly polarized pulse ionizes the He^+ via the single photon route, $|s,0\rangle\rightarrow|p,1\rangle$. $|s,0\rangle$ is the ground bound, and $|p,1\rangle$ is the continuum electron state with the magnetic quantum number $m=1$. Due to the perturbative limit, the ground state $|s,0\rangle$ still remains unchanged by the first laser pulse.[31] Then the second right-handed circularly polarized pulse ionizes the He^+ via the $|s,0\rangle\rightarrow|p,-1\rangle$. Due to the time delay between the two pulses, the initial electron wave packet will generate a phase of $e^{-iET_d/\hbar}$ by the first pulse, in which E represents the electron excess energy.[25] Therefore, the final superposition state with quantum numbers $m=\pm1$ reads[33]

$$|\psi_2\rangle\propto e^{-iET_d/\hbar}|p,1\rangle+|p,-1\rangle. \tag{6}$$

The interference of the states $|p,1\rangle$ and $|p,-1\rangle$ generates a vortex with c_2 rotational symmetry.[25]

For the photoionization, at wavelengths $\lambda_1=\lambda_2=40$ nm ($\omega_1=\omega_2=1.14$ a.u.), the corresponding angular frequencies ω_1 and ω_2 are below the ionization potential of the ground state of He^+. Thus, the ionization with a pair of left-right circularly polarized pulses proceeds via the two-photon route, $|s,0\rangle\rightarrow|p,1\rangle\rightarrow|d,2\rangle$ and $|s,0\rangle\rightarrow|p,-1\rangle\rightarrow|d,-2\rangle$, respectively. The generated electron wave function is

$$|\psi_4\rangle\propto e^{-iET_d/\hbar}|d,2\rangle+|d,-2\rangle, \tag{7}$$

which implies the vortex pattern having c_4 rotational symmetry as shown in Fig. 1(b). Analogously, the left-right circularly polarized laser pulses $\lambda_1=\lambda_2=90$ nm ($\omega_1=\omega_2=0.51$ a.u.) ionize the He^+ via the four-photon routes

$$|s,0\rangle\rightarrow|p,1\rangle\rightarrow|d,2\rangle\rightarrow|f,3\rangle\rightarrow|g,4\rangle,$$
$$|s,0\rangle\rightarrow|p,-1\rangle\rightarrow|d,-2\rangle\rightarrow|f,-3\rangle\rightarrow|g,-4\rangle,$$

and yield the final superposition state electron wave function

$$|\psi_8\rangle\propto e^{-iET_d/\hbar}|g,4\rangle+|g,-4\rangle. \tag{8}$$

The vortex pattern with c_8 rotational symmetry is shown in Fig. 1(c) which generated by the interference of the states $|g,4\rangle$ and $|g,-4\rangle$.

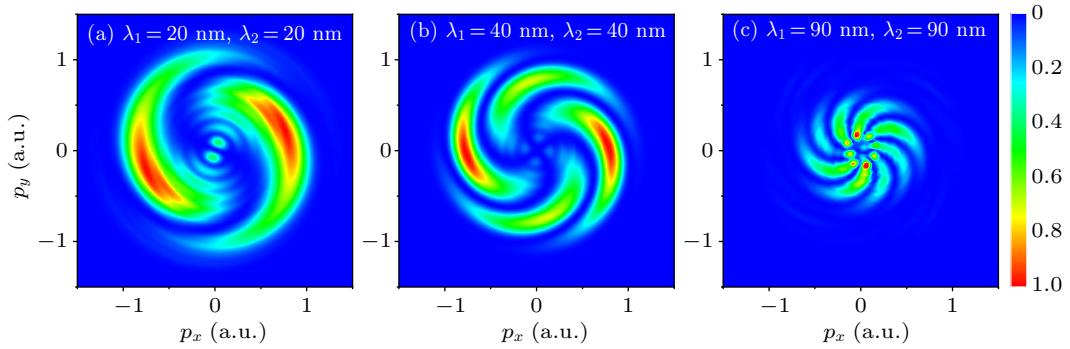


Fig. 1. The PMDs for the ground state as the initial electronic state of He^+ by a pair of left-right circularly polarized attosecond pulses at different wavelengths. (a) $\lambda_1 = \lambda_2 = 20$ nm, (b) $\lambda_1 = \lambda_2 = 40$ nm, (c) $\lambda_1 = \lambda_2 = 90$ nm. The time delay is $T_d = 3$ o.c.

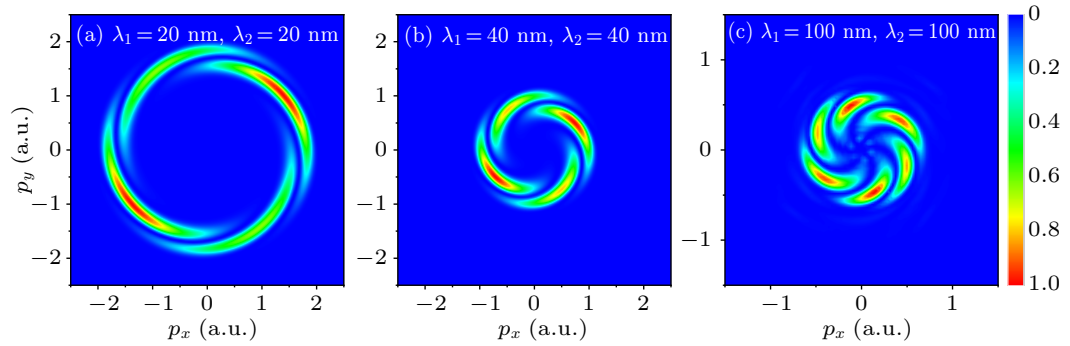


Fig. 2. The PMDs for the excited state as the initial electronic state of He^+ by a pair of left-right circularly polarized attosecond pulses at different wavelengths. (a) $\lambda_1 = \lambda_2 = 20$ nm, (b) $\lambda_1 = \lambda_2 = 40$ nm, (c) $\lambda_1 = \lambda_2 = 100$ nm. The time delay is $T_d = 3$ o.c.

We next show the signature of different spiral arms of the vortex pattern to discuss the dependence of the excited state as the initial electronic state on the PMDs, which is demonstrated in Fig. 2. It is found that the spiral arms of vortex patterns are four, four, and six as shown in Figs. 2(a)–2(c) at wavelengths $\lambda_1 = \lambda_2 = 20$ nm ($\omega_1 = \omega_2 = 2.28$ a.u.), $\lambda_1 = \lambda_2 = 40$ nm ($\omega_1 = \omega_2 = 1.14$ a.u.) and $\lambda_1 = \lambda_2 = 100$ nm ($\omega_1 = \omega_2 = 0.46$ a.u.) for the excited state as the initial electronic state. The time delay is $T_d = 3$ o.c.

According to the above discussion, the electrons in the excited state ($I_{P_2} = 0.5$ a.u.) can be ionized by absorbing one photon from every laser pulses ($\omega_1 = \omega_2 = 2.28$ a.u.) and generate the vortex pattern with two spiral arms. However, we see that the vortex pattern presents four spiral arms as illustrated in Fig. 2(a). The discrepancy in the spiral arms of the vortex patterns is originating from the difference of the initial electronic state. When the excited state is as the initial electronic state, the electron can be inoized from the first left-handed circularly polarized pulse via the single photon route, $|p,1\rangle \rightarrow |d,2\rangle$ and from the second right-handed circularly polarized pulse via the route, $|p,-1\rangle \rightarrow |d,-2\rangle$. The final state is the superposition of $|d,2\rangle$ state and $|d,-2\rangle$ state with quantum numbers $m = \pm 2$. It implies the vortex pattern with c_4 rotational symmetry, which is in agreement with the result as shown in Fig. 2(a). In analogy to the above discussion, the electrons can be ionized by the circularly polarized laser pulses $\lambda_1 = \lambda_2 = 40$ nm and present the vortex pattern with c_4 rotational symmetry as shown in Fig. 2(b). Of note is that the momentum of the ionized photoelectron shown in Fig. 2(b) is smaller than that shown in Fig. 2(a). It is because that the continuum electron momentum is $p = \sqrt{2(\omega - I_P)}$. For the single-photon ionization, the momentum of the ionized photoelectron is $p = 1.89$ a.u. at wavelengths $\lambda_1 = \lambda_2 = 20$ nm ($\omega_1 = \omega_2 = 2.28$ a.u.), and the momentum of the ionized photoelectron is $p = 1.13$ a.u. at wavelengths $\lambda_1 = \lambda_2 = 40$ nm ($\omega_1 = \omega_2 = 1.14$ a.u.). As shown in Fig. 2(c), at wavelengths $\lambda_1 = \lambda_2 = 100$ nm, the vortex pattern exhibits c_6 rotational symmetry, which is caused by the electrons ionization via the two-photon routes $|p,1\rangle \rightarrow |d,2\rangle \rightarrow |f,3\rangle$ and $|p,-1\rangle \rightarrow |d,-2\rangle \rightarrow |f,-3\rangle$.

To further understand the sensitivity of the initial electronic state on the vortex patterns in PMDs, the initial wave function of the different electronic states are illustrated in Fig. 3. The initial wave function of the ground state depicted in Fig. 3(a) shows all the electron density distribution locating in the central region. And the initial electron density distributions of the excited states as shown in Fig. 3(b) are mainly distributed in two regions of the first and third quadrants. With considering the interaction of He^+ in the excited states with a pair of attosecond pulses, the initial wave packets distributed in two regions create interference effects in the photoelectron spectra, which leads to two more spiral arms than in the ground state as the initial electronic state by absorbing the same number of photons. The characteristics of the vortex patterns [in

Figs. 1 and 2] agree well with the above analysis, indicating that the difference of initial electronic state causes the change in the vortex patterns in PMDs.

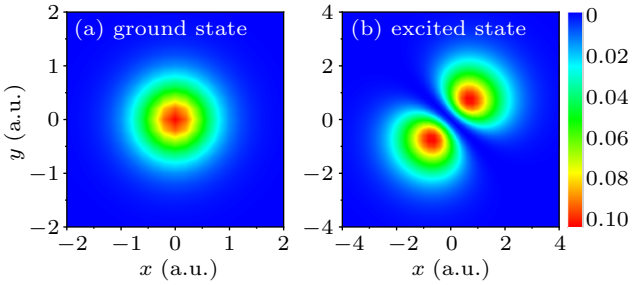


Fig. 3. Electron density distribution of (a) ground state and (b) excited state of He^+.

To compare the effect of the initial electronic state on PMDs, we select Figs. 1(b) and 2(b) to show the discrepancy. And the corresponding schematic energy-level diagram of Figs. 1(b) and 2(b) are illustrated in Figs. 4(a) and 4(b), respectively. As illustrated in Fig. 4(a), the vortex pattern with four spiral arms (Fig. 1(b)) can be generated by absorbing two-photon from the first laser pulse through path Γ_1, absorbing two-photon from the second laser pulse through path Γ_2, and absorbing a photon from different pulses through path Γ_{12} (or Γ_{21}).[24] The vortex pattern showed in Fig. 2(b) is generated by absorbing a photon from each of the two pulses through paths Γ_1 and Γ_2, which is shown in Fig. 4(b).

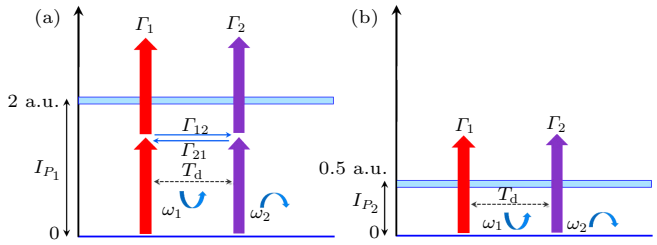


Fig. 4. Schematic energy-level diagrams for the ionization of He^+ in counter-rotating circularly polarized laser pulses delayed in time by T_d, in the case of (a) ground state and (b) excited state as the initial electronic state. The wavelengths of both pulses are $\lambda_1 = \lambda_2 = 40$ nm. The ionization pathways Γ_1 and Γ_2 are shown, respectively.

It can be found that the two vortex patterns are similar, and both exist the difference in the brightness (intensity of the PMDs). In Fig. 1(b), one sees that the two spiral arms along the horizontal axis have the same brightness, those two along its perpendicular direction are less bright; In Fig. 2(b), the intensities of the two spiral arms in the first and third quadrants are maximum. However, the intensities of the other two spiral arms in second and fourth quadrants are minimum. We note that the physical mechanisms which give rise to differences in distribution intensities are different. It is found that the difference in the brightness of the vortex patterns showed in Fig. 1(b) caused by the contribution of the ionization cross channel.[24] The authors in Ref. [24] first proposed the cross channel contributions and pointed out that the brightness of the vortex patterns depends on the time delay. However, the physical mechanism underlying the creation of the discrepancy in distribution shown in Fig. 2(b) is based on the initial electron density distribution. From Fig. 3(b) we get that the electron density distributions at the first and third quadrants are maximum, leading to larger momentum distributions in these regions than in others.

4. Conclusions

In summary, we have investigated the effects of the initial electronic state on vortex patterns in PMDs by a pair of counter-rotating circularly polarized attosecond pulses. Simulations are performed on He^+ by numerically solving the 2D TDSE. The initial electronic state plays an essential role in the PMDs. We demonstrate the effects of the initial electronic state on vortex patterns with varying wavelengths. It concludes that the number of spiral arms in vortex patterns is equal to the number of the absorbed photons when the initial state is the ground state. And the number of spiral arms in vortex patterns is always two more than the number of the absorbed photons when the initial state is the excited state. The initial electron density distributions are presented to interpret the difference of PMDs on the initial electronic state. Besides, we compare the PMDs of different initial electronic states with the same wavelengths. The results show that the vortex patterns in PMDs are similar. However, the physical mechanisms underlying the creation of the discrepancy in distribution are different. The study of different physical mechanisms can be employed to effectively control the distribution of electron vortices.

References

[1] Brabec T and Krausz F 2000 *Rev. Mod. Phys.* **72** 545
[2] Krausz F and Ivanov M 2009 *Rev. Mod. Phys.* **81** 163
[3] Chang Z and Corkum P 2010 *J. Opt. Soc. Am. B: Opt. Phys.* **27** B9
[4] Gaumnitz T, Jain A, Pertot Y, Huppert M, Jordan I, Ardana-Lamas F and Wörner H J 2017 *Opt. Express* **25** 27506
[5] Vrakking M J 2014 *Phys. Chem. Chem. Phys.* **16** 2775
[6] Chelkowski S, Yudin G and Bandrauk A 2006 *J. Phys. B: At. Mol. Opt. Phys.* **39** S409
[7] Niikura H, Villeneuve D and Corkum P 2005 *Phys. Rev. Lett.* **94** 083003
[8] Shao H C and Starace A F 2010 *Phys. Rev. Lett.* **105** 263201
[9] Du H, Zhang J, Ben S, Zhong H Y, Xu T T, Guo J and Liu X S 2016 *Chin. Phys. B* **25** 043202
[10] Xia C L and Miao X Y 2015 *Chin. Phys. Lett.* **32** 043202
[11] Zhang J, Qi T, Pan X F, Guo J, Zhu K G and Liu X S 2019 *Chin. Phys. B* **28** 103204
[12] Huang Y Y, Lai X Y and Liu X J 2018 *Chin. Phys. B* **27** 073204
[13] Feng L Q and Liu H 2015 *Chin. Phys. B* **24** 034206
[14] Shao J, Zhang C P, Jia J C, Ma J L and Miao X Y 2019 *Chin. Phys. Lett.* **36** 054203
[15] Ben S, Guo P Y, Song K L, Xu T T, Yu W W and Liu X S 2017 *Opt. Express* **25** 1288
[16] Ben S, Guo P Y, Pan X F, Xu T T, Song K L and Liu X S 2017 *Chem. Phys. Lett.* **679** 38
[17] Li B Q, Ren X H and Zhang J T 2020 *Chin. Phys. B* **29** 043202
[18] Jia X Y, Fan D H, Li W D and Chen J 2013 *Chin. Phys. B* **22** 013303
[19] Wu W Y and He F 2016 *Phys. Rev. A* **93** 023415

[20] Zhang H D, Ben S, Xu T T, Song K L, Tian Y R, Xu Q Y, Zhang S Q, Guo J and Liu X S 2018 *Phys. Rev. A* **98** 013422
[21] Yuan K J, Chelkowski S and Bandrauk A D 2015 *Chem. Phys. Lett.* **638** 173
[22] Cui H F and Miao X Y 2020 *Chin. Phys. B* **29** 074203
[23] Yuan K J, Chelkowski S and Bandrauk A D 2014 *Chem. Phys. Lett.* **592** 334
[24] Djiokap J M N, Meremianin A V, Manakov N. L, Hu S X, Madsen L B and Starace A F 2016 *Phys. Rev. A* **94** 013408
[25] Djiokap J M N, Hu S X, Madsen L B, Manakov N L, Meremianin A V and Starace A F 2015 *Phys. Rev. Lett.* **115** 113004
[26] Zhen Q, Zhang H D, Zhang S Q, Ji L, Han T and Liu X S 2020 *Chem. Phys. Lett.* **738** 136885
[27] Li M, Zhang G Z, Ding X and Yao J Q 2019 *Chin. Phys. Lett.* **36** 063201
[28] Yuan K J, Lu H Z and Bandrauk A D 2017 *J. Phys. B: At. Mol. Opt. Phys.* **50** 124004
[29] Yuan K J, Chelkowski S and Bandrauk A D 2016 *Phys. Rev. A* **93** 053425
[30] Li M, Zhang G Z, Kong X L, Wang T Q, Ding X and Yao J Q 2018 *Opt. Express* **26** 878
[31] Li M, Zhang G Z, Zhao T Q, Ding X and Yao J Q 2017 *Chin. Opt. Lett.* **15** 120202
[32] Pengel D, Kerbstadt S, Johannmeyer D, Englert L, Bayer T and Wollenhaupt M 2017 *Phys. Rev. Lett.* **118** 053003
[33] Pengel D, Kerbstadt S, Englert L, Bayer T and Wollenhaupt M 2017 *Phys. Rev. A* **96** 043426
[34] Xiao X R, Wang M X, Liang H, Gong Q H and Peng L Y 2019 *Phys. Rev. Lett.* **122** 053201
[35] Feit M D, Fleck Jr J A and Steiger A 1982 *J. Comput. Phys.* **47** 412
[36] He P L, Takemoto N and He F 2015 *Phys. Rev. A* **91** 063413